Macromolecules

pubs.acs.org/Macromolecules Article

Ultralow Dielectric Constant Films from the Polyisoprene Modified with Dual Functions of Benzocyclobutene and Vinyl Groups

Chengcheng Zhou, Ding Shen, Boyang Shi, Xiaotong Fang, Xingpeng Chai, and Guowei Wang*

Cite This: *Macromolecules* 2025, 58, 13373−13381 Read Online

ACCESS | Metrics & More | Article Recommendations | Supporting Information

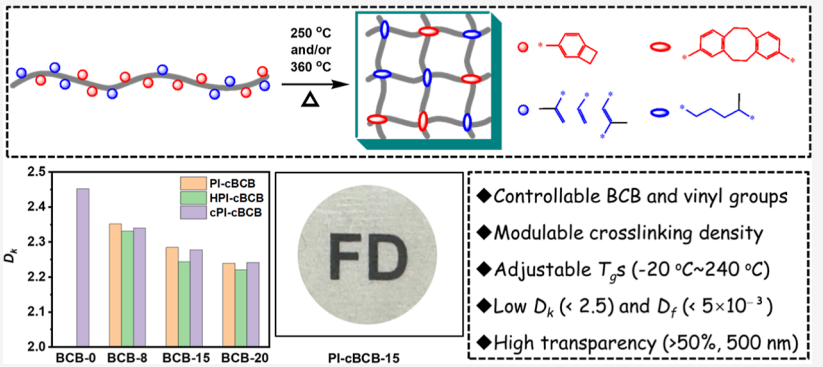

ABSTRACT: The rapid advancement of the semiconductor industry has imposed heightened demands on interlayer insulating dielectric materials to meet varying processing requirements. In this contribution, a series of polyolefin-based low-*k* materials were developed by integrating dual functional groups of benzocyclobutene (BCB) and vinyl together through grafting the BCB group onto the polyisoprene (PI) mainchain. As a comparison, the PI mainchain was also selectively modified as a hydrogenated PI (HPI) counterpart. Both the introduced BCB and the remaining vinyl groups on PI could be selectively cured at 250 and 360 °C, respectively. Notably, with the increase of BCB group contents, the storage moduli, tan δ, and glass transition temperature (T_g) of the cured samples were regularly enhanced, and the coefficients of thermal expansion (CTE) values were correspondingly decreased. Especially, by modulating the curing behavior of BCB and/or vinyl groups, the T_gs could be tailored across a broad range (29 to 240 °C), ensuring adaptability to diverse processing conditions. As expected, the polyolefin-based materials exhibit exceptional dielectric performance with all film samples demonstrating a dielectric constant (D_k) < 2.5 and dielectric loss (D_f) < 5 × 10^{-3} (at 1 MHz). This work illustrated that the PI modified with dual functions of BCB and vinyl groups possessed significant potential as a low-*k* material for future versatile, integrated circuit applications.

INTRODUCTION

Low-dielectric constant (D_k) materials are pivotal in microelectronics, electronic packaging, and high-frequency 5G communication systems due to their critical role in minimizing signal delay and energy loss caused by resistance-capacitance (RC) coupling effects.[1−5] As device miniaturization and operating frequencies escalate, traditional dielectric materials, such as silica (D_k ≈ 3.9−4.2) and polyimides (D_k ≈ 3.0−3.5), face limitations in meeting the stringent requirements for ultralow dissipation factor (D_f < 5 × 10^{-3}) and thermal management in high-frequency regimes.[6−8] Modern low-*k* materials must simultaneously satisfy multiple performance criteria: low dielectric constants, high glass transition temperatures (T_g), robust mechanical strength, low moisture absorption, and thermal expansion coefficients (CTE) compatible with copper interconnects.[9,10]

To address these requirements, researchers have developed low-*k* materials through three primary strategies: (1) incorporation of fluorine atoms or other electronegative elements to reduce molecular polarizability by lowering electron cloud density;[11−14] (2) fabrication of porous architectures via templating or phase-separation techniques, where introduced air voids (D_k ≈ 1) effectively decrease the overall dielectric constant;[15−18] and (3) introduction of bulky functional groups or sterically hindered substituents to inhibit chain packing and suppress dipole polarization.[19−23] These approaches synergistically minimize both electronic and orientation polarization contributions, thereby achieving ultralow-*k* values while maintaining essential mechanical and thermal properties.

Received: October 16, 2025
Revised: November 17, 2025
Accepted: November 28, 2025
Published: December 9, 2025

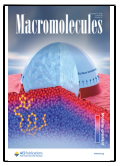

https://doi.org/10.1021/acs.macromol.5c02864
Macromolecules 2025, 58, 13373−13381

Scheme 1. Schematic Illustration of the Synthetic Procedure for BCB-Functionalized Polyolefins and the Curing Process for Low-*k* Films

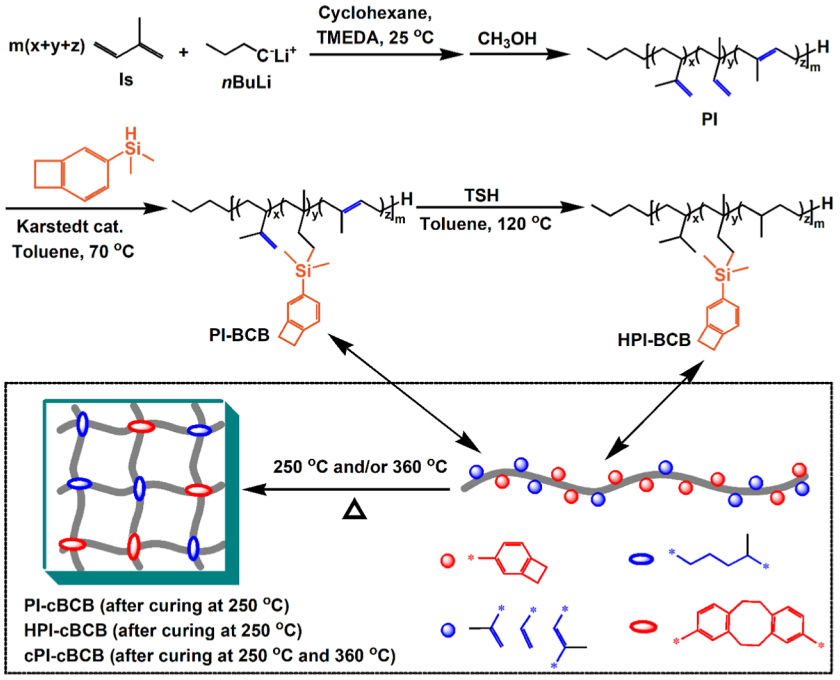

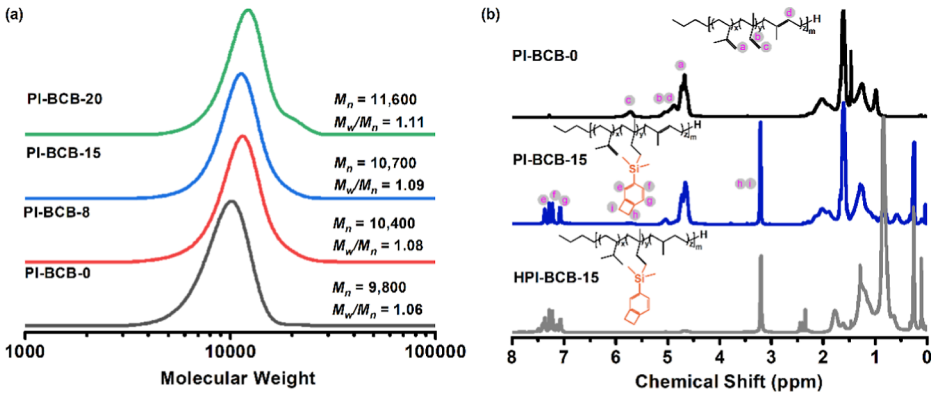

Figure 1. (a) SEC traces for PI-BCB samples (using THF as elution and polystyrene (PS) as standard), (b) ^{1}H NMR spectra of PI-BCB-0, PI-BCB-15, and HPI-BCB-15 (in $CDCl_3$).

Based on these strategies, polyolefins emerge as a highly promising material platform for low-*k* applications due to their inherent chemical structure. The saturated C−C and C−H bonds result in minimal molecular polarity, providing a naturally low dielectric constant.[24−26] For example, using cyclic olefin copolymers (COCs), the researchers have garnered significant attention in the low-*k* dielectric field owing to their inherent nonpolarity, tunable porosity, and compatibility with scalable manufacturing processes.[27−29] The polyolefin-derived low-*k* materials were also successfully synthesized through nanostructuring (*e.g.*, controlled pore architectures < 50 nm) and hybridization with low-polarity fillers (*e.g.*, silica nanoparticles), effectively addressing the historical limitations of poor mechanical strength in conventional polyolefins.[30−33] Complementing these academic endeavors, the industrial applications of polyolefin-based low-*k* materials have been notably advanced through the commercialization of COCs. A prominent example is Mitsui Chemicals' APEL series, which leverages the intrinsic material properties of COCs—such as ultralow water absorption, high purity, and excellent electrical insulation—to meet the stringent requirements of high-frequency applications like 5G infrastructure and millimeter-wave components. Furthermore, the cross-linked thermoset polyolefin counterparts were also successfully developed as dielectric layers in advanced copper-clad laminates, offering an optimal balance of low dielectric loss, thermal resistance, and mechanical stability. These industrial solutions validate the transition of polyolefin innovations from laboratory research to market-ready applications, with ongoing development efforts focused on further enhancing their thermal and interfacial properties for next-generation electronics. Nevertheless, the relatively high D_k of around 3.5 of these modified systems remains a critical barrier to their adoption in high-performance electronic devices. Meanwhile, the broader applications of polyolefins in advanced electronics are hampered by their intrinsic thermo-mechanical limitations.[34] Specifically, their relatively low thermal deformation temperature and pronounced creep

https://doi.org/10.1021/acs.macromol.5c02864
Macromolecules 2025, 58, 13373−13381

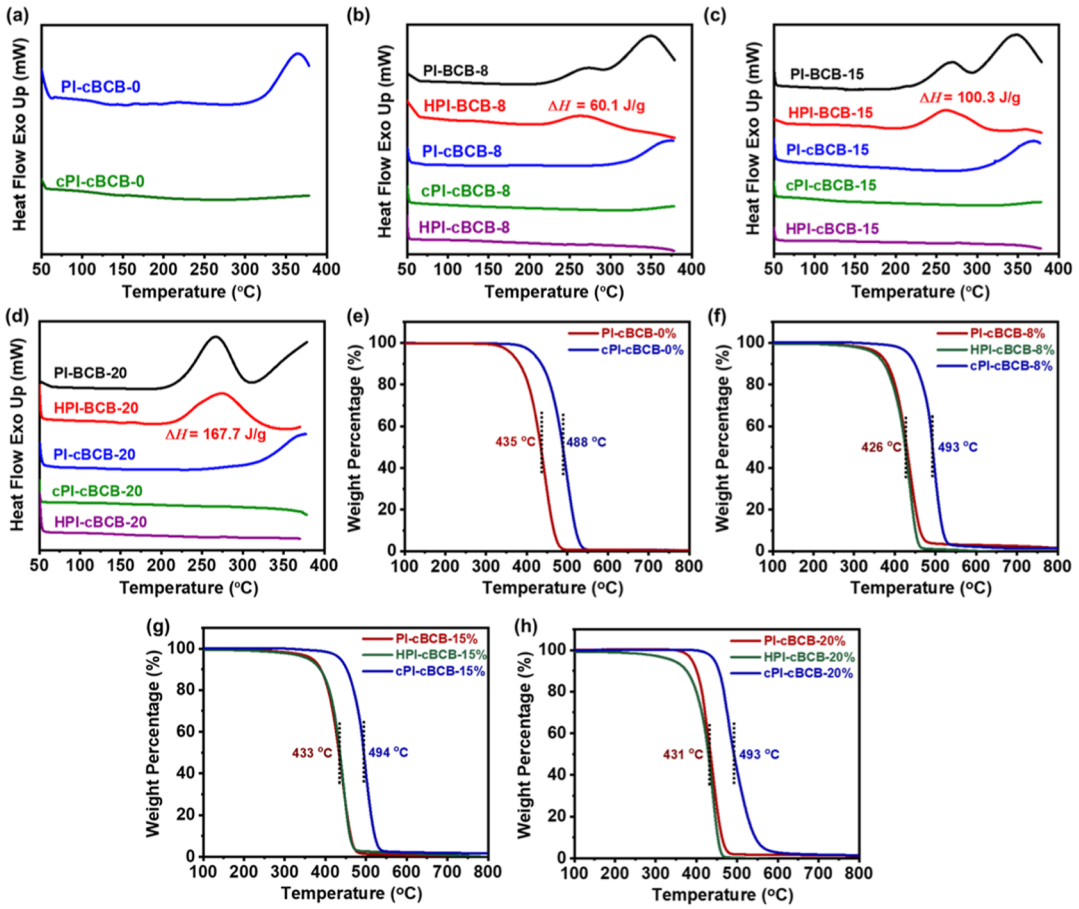

Figure 2. DSC traces for (a) PI-BCB-0 and HPI-BCB-0, (b) PI-BCB-8 and the derivatives, (c) PI-BCB-15 and the derivatives, and (d) PI-BCB-20 and the derivatives. TGA curves for (e) PI-BCB-0 and HPI-BCB-0, (f) PI-BCB-8 and the derivatives, (g) PI-BCB-15 and the derivatives, and (h) PI-BCB-20 and the derivatives.

behavior under sustained stress raise concerns regarding long-term reliability in demanding operating environments. Thus, comprehensively improving the k value and thermal stability of polyolefins is still urgent for future practical application.

In this contribution, an alternative strategy was developed for the polyolefin-based low-k materials. In detail, the polyisoprene (PI) precursor was first synthesized via living anionic polymerization (LAP), and the benzocyclobutene (BCB) moieties were grafted onto the PI backbone for BCB-functionalized polyolefins through a selective hydrosilylation reaction on the highly reactive1,2-addition unit. The remaining vinyl groups on the PI mainchain were further modified for hydrogenated PI (HPI). Subsequently, the BCB group and the remaining vinyl groups on PI were selectively cross-linked at 250 and 360 °C, respectively, offering the cured polyolefins with low-k values, adjustable cross-linking density, and T_g. The curing behavior and thermomechanical and dielectric properties of the resulting materials were systematically monitored using differential scanning calorimetry (DSC), thermogravimetric analysis (TGA), thermomechanical analysis (TMA), and dynamic mechanical analysis (DMA), respectively.

RESULTS AND DISCUSSION

Synthesis and Characterization of BCB-Functionalized Polyolefins. As illustrated in Scheme 1, the PI precursor with a narrow molecular weight distribution (M_w/M_n) of 1.07 (Figure 1a) was first prepared via an LAP process. Subsequently, a hydrosilylation reaction was performed between the unsaturated double bonds (1,2-addition unit on PI) and the presynthesized (benzocyclobutene-4-yl) dimethylsilane (BCB−SiH) in the presence of a Karstedt catalyst, and the PI-BCB samples were obtained. The successful incorporation of the BCB group onto the PI mainchain was ascertained by size exclusion chromatography (SEC) measurement with the monomodal peaks and low M_w/M_n values, confirming the absence of side reactions on the PI mainchain during the hydrosilylation reaction process (Figure 1a). Also, the PI-BCB samples were confirmed by proton nuclear magnetic resonance (^{1}H NMR) analysis. As shown in Figure 1b, the characteristic resonance signals for the vinyl protons from 1,2-(δ = 5.71 ppm), 3,4-(δ = 4.65 ppm), and 1,4-addition (δ = 5.04 ppm) units on the PI mainchain could be well discriminated from the spectrum for PI-BCB-0. By integrating the areas for vinyl protons, the molar percentages of 1,2-, 3,4-, and 1,4-addition units in precursor PI have been determined as 18.7%, 16.7%, and 64.6%, respectively. After the introduction of the BCB group, the characteristic resonance signals for the BCB cyclobutane protons (δ = 3.18 ppm) and aromatic protons (δ = 6.90−7.04 ppm) were also well discriminated from the spectrum for PI-BCB-15. By changing the feed molar ratio of BCB-SiH to the PI mainchain, the BCB group contents on the final PI-BCB samples could be modulated. As shown in Figure S1, with the increase of the degree of BCB functionalization, the resonance signals at 3.18 and 6.90−

https://doi.org/10.1021/acs.macromol.5c02864
Macromolecules 2025, 58, 13373−13381

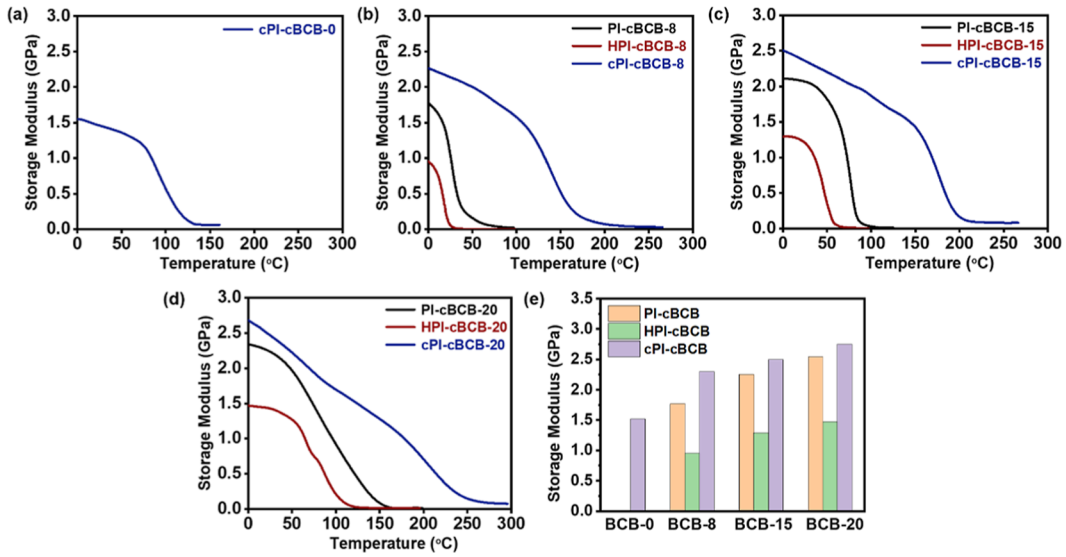

Figure 3. Storage moduli curves for (a) cPI-cBCB-0; (b) PI-cBCB-8, HPI-cBCB-8, and cPI-cBCB-8; (c) PI-cBCB-15, HPI-cBCB-15, and cPI-cBCB-15; and (d) PI-cBCB-20, HPI-cBCB-20, and cPI-cBCB-20. (e) Comparison of storage moduli values for samples with different BCB group contents.

7.04 ppm attributed to the cyclobutane and aromatic protons on the BCB group were regularly increased, while the resonance signal at 5.71 ppm was regularly decreased, confirming the selective hydrosilylation reaction of vinyl groups on the 1,2-addition unit on the PI mainchain. The integration of these protons quantified the degree of BCB functionalization as 8, 15, and 20 mol/100 g, respectively, which resembled the typical expression of the epoxy value in literature.[35] Thus, the PI-BCB samples were correspondingly termed as PI-BCB-8, PI-BCB-15, and PI-BCB-20, respectively. For consistent expression, the sample without the BCB group, *i.e.*, the PI precursor, was termed as PI-BCB-0. Notably, the hydrosilylation reaction selectively happened with vinyl group on 1,2-addition unit on precursor PI, thus, the maximum degree of BCB functionalization was around 20 mol/100 g.

Furthermore, referring to the literature,[36] the PI-BCB samples were subjected to a hydrogenation reaction in the presence of 4-methylbenzenesulfonhydrazide (TSH) using xylene as a solvent at 135 °C. The complete hydrogenation was verified by the complete disappearance of resonance signals of vinyl protons between 4.65 and 5.71 ppm in the ^{1}H NMR spectra for HPI-BCB-15 (Figure 1b), while the BCB-specific resonance signal at 3.18 ppm and 6.90−7.04 ppm remained intact, confirming the retention of BCB functionality. Correspondingly, the hydrogenated samples were termed as HPI-BCB-8, HPI-BCB-15, and HPI-BCB-20, respectively. It should be noted that, in the following section, HPI-BCB-0 was out of the discussion due to the absence of any BCB and vinyl groups, exhibiting as a liquid state.

Curing Behavior of BCB-Functionalized Polyolefins. To investigate the curing behavior of the obtained PI-BCB and HPI-BCB samples, the samples before and after the curing were comprehensively characterized and compared by DSC measurement with a heating rate of 10 °C min^{-1} under a nitrogen atmosphere over a temperature range of 50−380 °C. For convenience, in the following section, the PI cured by the cross-linking of vinyl groups was termed as cPI, and that cured by the cross-linking of the BCB group was termed as cBCB. As shown in Figure 2a−d, during the first heating run, all the PI-BCB-8, PI-BCB-15, and PI-BCB-20 samples exhibited an exothermic peak at 268 °C corresponding to the curing of BCB group and an exothermic peak at 348 °C corresponding to the curing of vinyl groups on the PI mainchain, which was consistent with the curing temperature reported in our previous work.[37] As a comparison, for PI-BCB-0, only an exothermic peak at 348 °C can be detected, confirming the sole curing of the vinyl groups on the PI mainchain. After the hydrogenation reaction, all of the HPI-BCB-8, HPI-BCB-15, and HPI-BCB-20 samples showed a single exothermic peak at 268 °C corresponding to the curing of BCB group during the first heating run, meanwhile confirming the complete hydrogenation of samples. Additionally, with the increase of BCB group contents, the curing enthalpies of 60.1 J/g, 100.3 J/g, and 167.7 J/g were derived for HPI-BCB-8, HPI-BCB-15, and HPI-BCB-20 samples, respectively.

Furthermore, by setting the curing process at 250 °C, the BCB group was cured, and the vinyl groups on the PI mainchain remained. The obtained PI-cBCB-0, PI-cBCB-8, PI-cBCB-15, and PI-cBCB-20 samples were also monitored by DSC measurements during the first heating run. From 325 °C, a rising tendency could be discriminated for the DSC curves of corresponding PI-cBCB-0, PI-cBCB-8, PI-cBCB-15, and PI-cBCB-20 samples, confirming the further curing of vinyl groups on the PI mainchain. Alternatively, by setting the curing process at 360 °C, all the BCB group and the vinyl groups on the PI mainchain would be cured. Thus, for all the cPI-cBCB-0, cPI-cBCB-8, cPI-cBCB-15, cPI-cBCB-20, HPI-cBCB-8, HPI-cBCB-15, and HPI-cBCB-20 samples, no exothermic peaks could be discriminated from DSC curves during the first heating run, confirming that all the BCB and vinyl groups on PI had been completely consumed and the samples had been successfully cured.

Additionally, the thermal properties of the cured BCB-functionalized polyolefins were also evaluated by TGA with a heating rate of 10 °C min^{-1} under a nitrogen atmosphere over a temperature range of 50−800 °C (Figure 2e−h). Typically, the 5% weight loss temperature (T_{5d}) was especially emphasized in literature due to its reflection on the thermal stability of materials.[38,39] From PI-cBCB-8, PI-cBCB-15, to PI-cBCB-20, the T_{5d} progressively increased from 359 °C, 368 °C,

https://doi.org/10.1021/acs.macromol.5c02864
Macromolecules 2025, 58, 13373−13381

Table 1. Data for PI-cBCB, HPI-cBCB, and cPI-cBCB Samples Evaluated by Different Measurements

entry	samples[a]	BCB group contents (mol/100 g)[b]	DMA		TMA
			storage modulus at 0 °C[a] (GPa)[c]	T_g (°C)[d]	CTE (ppm/°C)[e]
1	PI-cBCB-8	8	1.78	36	86.68
2	PI-cBCB-15	15	2.11	84	78.39
3	PI-cBCB-20	20	2.34	135	66.57
4	HPI-cBCB-8	8	0.95	29	96.59
5	HPI-cBCB-15	15	1.29	64	82.13
6	HPI-cBCB-20	20	1.47	109	71.83
7	cPI-cBCB-0	0	1.52	132	80.14
8	cPI-cBCB-8	8	2.26	169	73.52
9	cPI-cBCB-15	15	2.50	203	54.21
10	cPI-cBCB-20	20	2.68	240	60.06

[a]The PI mainchain cured by cross-linking of the vinyl group was termed as cPI, and that cured by cross-linking of the BCB group was termed as cBCB. [b]The BCB group contents were calculated according to the ^{1}H NMR spectra, and the values were defined as the molarity of BCB groups per 100 g sample. [c]The storage moduli values were evaluated as the data at 0 °C, which was collected by the DMA measurement with a heating rate of 3 °C min^{-1} under a nitrogen atmosphere in a temperature range of −50−300 °C. [d]The T_g values were evaluated as the peak temperature in tan δ curves, which were collected by DMA measurement with a heating rate of 3 °C min^{-1} under a nitrogen atmosphere in a temperature range of −50−300 °C. [e]The CTE values were evaluated by TMA measurement with a heating rate of 10 °C min^{-1} under a nitrogen atmosphere in a temperature range of −50−300 °C.

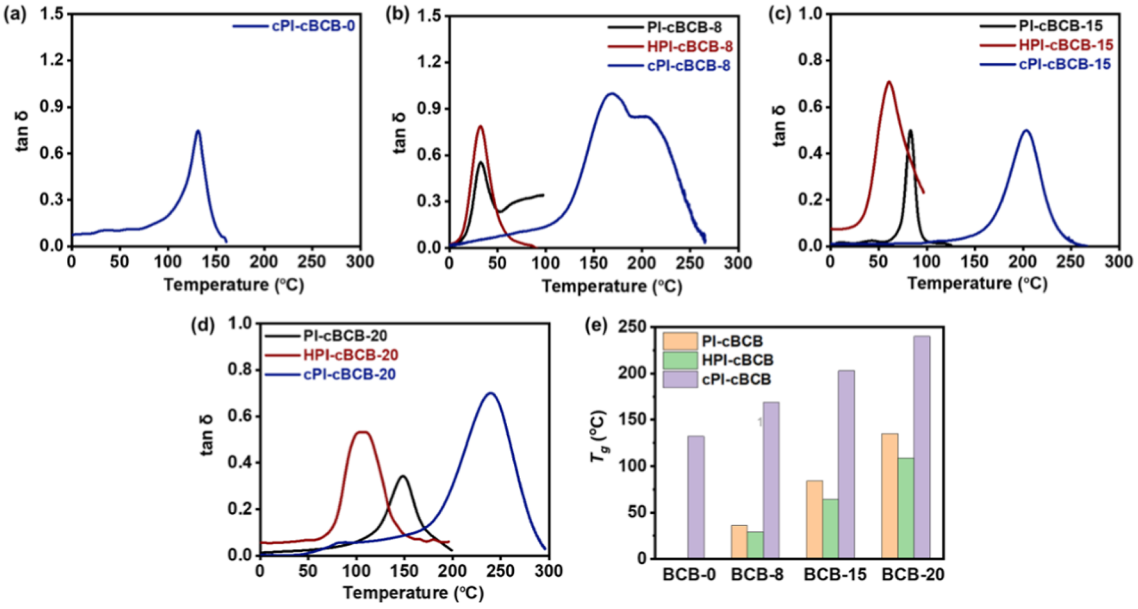

Figure 4. Tan δ curves for (a) cPI-cBCB-0; (b) PI-cBCB-8, HPI-cBCB-8, and cPI-cBCB-8; (c) PI-cBCB-15, HPI-cBCB-15, and cPI-cBCB-15; and (d) PI-cBCB-20 HPI-cBCB-20, and cPI-cBCB-20. (e) Comparison of T_gs values for samples with different BCB group contents.

to 387 °C, respectively, as the BCB group contents increased (Figure 2f−h). Similarly, a consistent trend was also observed for the hydrogenated counterparts, where HPI-cBCB-8, HPI-cBCB-15, and HPI-cBCB-20 exhibited T_{5d} values of 342 °C, 349 °C, and 358 °C, respectively (Figure 2f−h). Comparative analysis between the TGA curves for PI-cBCB and HPI-cBCB samples revealed a slight reduction in T_{5d} after hydrogenation, suggesting that the hydrogenation marginally diminishes the thermal stability, potentially attributable to the possible cross-linking effect associated with double bonds. Remarkably, the cPI-cBCB series exhibited a significant increase in T_{5d}, with values of 430 °C, 432 °C, 436 °C, and 444 °C for cPI-cBCB-0, cPI-cBCB-8, cPI-cBCB-15, and cPI-cBCB-20, respectively (Figure 2e−h). Meanwhile, the maximum decomposition rate temperatures of the cPI-cBCB series were about 50−60 °C higher than those of the PI-cBCB and HPI-cBCB series, attributed to the increased cross-linking density resulting from the curing of the residual vinyl groups on PI.

Mechanical Properties of the Cured BCB-Functionalized Polyolefins. The mechanical properties of the cured BCB-functionalized polyolefins were investigated via DMA with a heating rate of 3 °C min^{-1} under a nitrogen atmosphere over a temperature range of −50−300 °C. As shown in Figure 3a−d and Table 1, the storage moduli values measured at 0 °C for the PI-cBCB-8, PI-cBCB-15, and PI-cBCB-20 samples with varying BCB group contents were 1.78, 2.11, and 2.34 GPa, respectively; hydrogenated counterparts of HPI-cBCB-8, HPI-cBCB-15, and HPI-cBCB-20 samples exhibited reduced storage moduli values of 0.95, 1.29, and 1.47 GPa, respectively. Uniquely, the cPI-cBCB-0, cPI-cBCB-8, cPI-cBCB-15, and cPI-cBCB-20 samples demonstrated enhanced storage moduli values of 1.52, 2.26, 2.50, and 2.68 GPa, respectively. Regularly, the rigidity of the cured PI-cBCB, HPI-cBCB, and cPI-cBCB

https://doi.org/10.1021/acs.macromol.5c02864
Macromolecules 2025, 58, 13373−13381

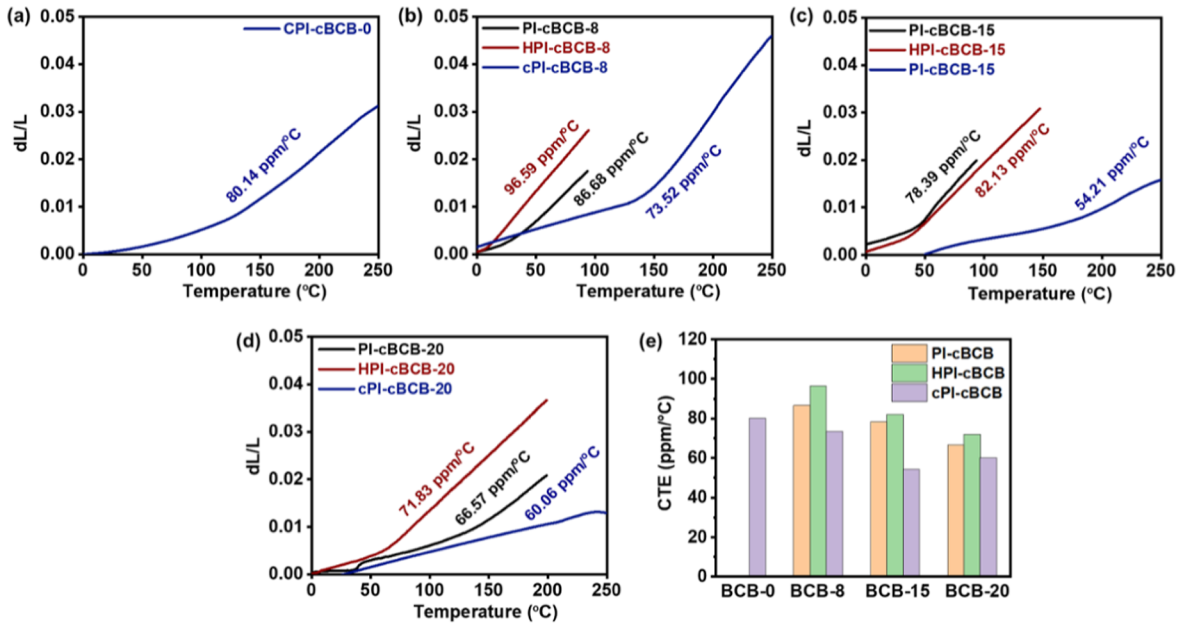

Figure 5. TMA curves for (a) cPI-cBCB-0; (b) PI-cBCB-8, HPI-cBCB-8, and cPI-cBCB-8; (c) PI-cBCB-15, HPI-cBCB-15, and cPI-cBCB-15; and (d) PI-cBCB-20 HPI-cBCB-20, and cPI-cBCB-20. (e) Comparison of CTE values for samples with different BCB group contents.

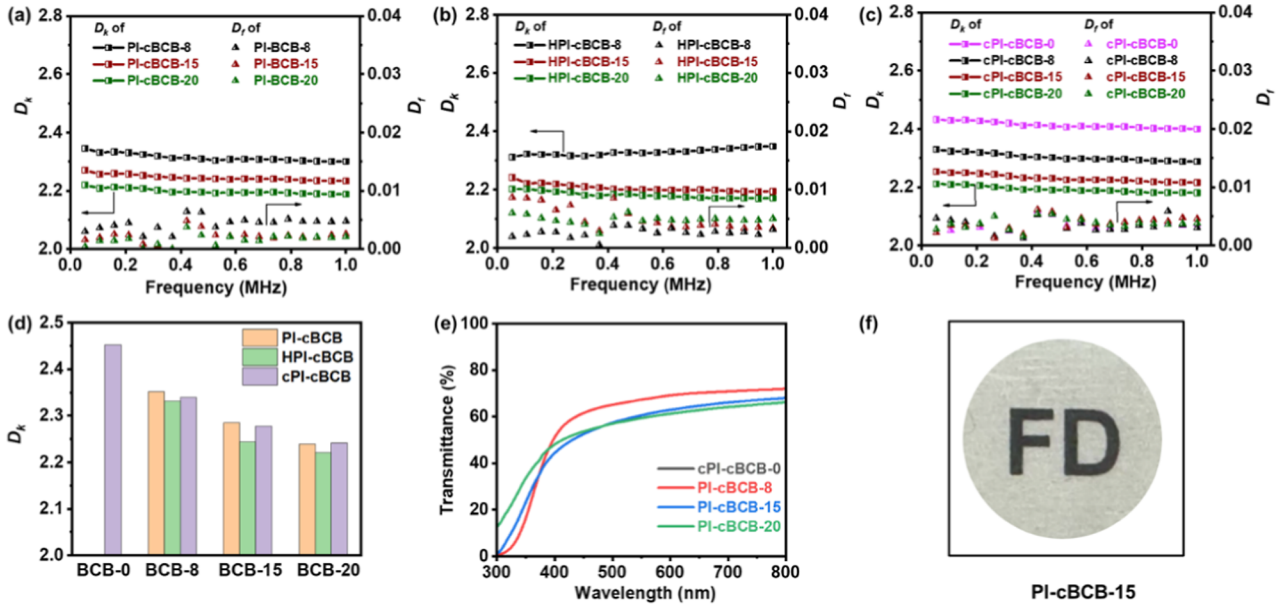

Figure 6. D_k and D_f of (a) PI-cBCB-8, PI-cBCB-15, and PI-cBCB-20; (b) HPI-cBCB-8, HPI-cBCB-15, and HPI-BCB-20; and (c) cPI-cBCB-0, cPI-cBCB-8, cPI-cBCB-15, and cPI-cBCB-20. (d) Comparison of D_k values for samples with different BCB group contents. (e) UV−vis spectra for cPI-cBCB-0, PI-cBCB-8, PI-cBCB-15, and PI-cBCB-20 with a film thickness around 0.10 mm. (f) Photo of the PI-cBCB-15 film on a "FD" letters.

samples increased progressively with the increase of BCB group contents (Figure 3e). Especially, the cross-linking of the vinyl groups on the PI mainchain further elevated cross-linking density beyond BCB-induced networks. However, the hydrogenation diminished stiffness, imparting flexibility that mitigates inherent brittleness. The T_gs determined from temperature-dependent tan δ profiles showed the similar tendency (Figure 4a−d and Table 1). That is, the PI-cBCB-8, PI-cBCB-15, and PI-cBCB-20 samples registered T_gs at 36 °C, 84 °C, and 135 °C, respectively; the corresponding hydrogenated versions of HPI-cBCB, HPI-cBCB, and HPI-cBCB-20 samples showed T_gs at 29 °C, 64 °C, and 109 °C, respectively. The cPI-cBCB-0, cPI-cBCB-8, cPI-BCB-15, and cPI-cBCB-20 samples reached T_gs at 132 °C, 169 °C, 203 °C, and 240 °C, respectively. Furthermore, the quantitative cross-linking densities of all BCB-based polyolefins are calculated and summarized in Table S1. The T_g and cross-linking density have a consistent tendency, which is actually tunable. Again, these results demonstrated that the strategic manipulation of BCB group contents, coupled with selective hydrogenation or further curing of vinyl groups, enabled modulable cross-linking density and precise T_g tuning across a 211 °C range (29−240 °C), facilitating material customization for diverse applications (Figure 4e).

Additionally, the dimensional stability constitutes a critical performance metric for low-k materials in integrated circuit

https://doi.org/10.1021/acs.macromol.5c02864
Macromolecules 2025, 58, 13373−13381

applications,[40] evaluated via TMA with a heating rate of 10 °C min^{-1} under a nitrogen atmosphere across a temperature range of −50−300 °C. The CTE values were determined by calculating the average dL/L value over the temperature range from 0 °C to the inflection point (*i.e.*, T_g), illustrated in Figure 5a−d, summarized in Table 1, and depicted in Figure 5e. All of the cured samples exhibited exceptional thermal expansion behavior. Comparatively, the HPI-cBCB samples had the highest CTE values. The cPI-cBCB samples with significantly enhanced cross-linking density achieved through cross-linking of both vinyl and BCB groups markedly reduced the CTE values, effectively suppressing chip warpage in advanced electronic packaging. Obviously, the tendency of CTE values was consistent with the above storage modulus, tan δ, and T_gs evaluated by DMA measurement.

Dielectric Properties of the Cured BCB-Functionalized Polyolefins. The dielectric constant (D_k) and dissipation factor (D_f) of the cured films with a thickness around 0.10 mm were measured using an impedance analyzer at 25 °C over a frequency range of 1 Hz to 1 MHz. As shown in Figure 6a−c, all samples exhibited D_k values below 2.5 and D_f values below 5×10^{-3}, demonstrating a notable advantage over commercially available polyolefin-based low-k materials. Regularly, it was observed that as the BCB group contents in the PI-cBCB, HPI-cBCB, and cPI-cBCB samples increased, the D_k progressively decreased. Comparatively, cPI-BCB-0 without BCB group showed the highest D_k value, confirming that the BCB group had a prominent effect on the dielectric properties. For samples with identical BCB content, the hydrogenation slightly improved the dielectric properties of HPI-cBCB samples. This could be attributed to the fact that the originally present C═C double bonds in the polymer possess a π-electron cloud that was relatively easily polarized. After hydrogenation, these π-bonds were cleaved and transformed into new σ-bonds, which exhibited lower polarizability compared to π-bonds, consequently reducing the overall dielectric constant of the polymer. The HPI-cBCB-20 sample exhibited the lowest D_k value of 2.22 at 1 MHz with an average $D_f < 4 \times 10^{-3}$. The D_k curve of the HPI-cBCB-8 sample displayed an unusual upward trend, which might be attributed to its higher elasticity, resulting in variations in material thickness during testing. Comprehensively, based on these findings, it could be inferred that the introduction of BCB group and the hydrogenation process were key factors governing the dielectric performance of polyolefin-based low-k materials.

However, minimal change in the dielectric properties of the samples before and after cross-linking of vinyl groups on the PI mainchain could be discriminated. This might be because the cross-linking of BCB groups already effectively restricted segmental motion of the mainchain and rotation of dipoles. Therefore, further increases in cross-linking density have limited impact on improvement of the dielectric properties. Nevertheless, as confirmed in the above section, further increases in cross-linking density would significantly increase the T_gs and decrease the CTE values of samples. Combined with the increased T_gs and decreased CTE, as well as the optimized D_k and D_f, the modification of polyolefins exhibited versatile potential in a low-k material field. Prominently, the dielectric properties and thermal properties of polyolefin-based low-k material developed in this work are superior to the reports in several literature studies (Table S2).

Additionally, from Figures 6e and 6f, it can be observed that the cPI-BCB-0 has the highest transmittance in the visible light region (≥400 nm). The introduction of BCB group slightly decreased the transmittance of the cured films. Nevertheless, the PI-cBCB-8, PI-cBCB-15, and PI-cBCB-20 films still retained high transparency, confirmed by the clear observation of the "FD" letters below the PI-cBCB-15 film. Furthermore, to evaluate the long-term stability of low-k material, the D_f and D_k of cPI-cBCB samples after six months were remeasured and compared with those of the previous as-synthesized samples (Figure S2). The D_k values of samples before and after six months were almost overlapped, and the D_f values were slightly affected, confirming the excellent long-term stability of the polyolefin-based low-k material. Additionally, sing PI-BCB-20 as an example, the PI-cBCB-20 film on a silicon wafer was subjected to a preliminary adhesion test. No delamination or removal of the material was observed after the tape was peeled off, suggesting good adhesion to the silicon substrate (Figure S3). With these advantages, it is hoped that the high transmittance, long-term stability, and excellent adhesion ability will further facilitate the polyolefin films as extensive applications in advanced materials.

CONCLUSIONS

In summary, based on the selective reaction of BCB-SiH and the vinyl group on the 1,2-addition unit, the PI-BCB samples with controlled BCB group contents were readily synthesized. Also, the PI mainchain could be selectively hydrogenated as an HPI mainchain for HPI-BCB samples. By selective curing of the BCB group at 250 °C and vinyl groups at 360 °C, the PI-BCB and HPI-BCB could be selectively cured, and the PI-cBCB, cPI-cBCB, and HPI-cBCB were obtained. The DMA results showed that the storage moduli, tan δ, and T_gs of the cured samples were regularly enhanced with the increase of BCB group contents. The TMA results showed that the CTE values were correspondingly decreased with the increase of BCB group contents. Uniquely, the cross-linking density and the corresponding T_gs could be tailored across a broad range (29 to 240 °C) by modulating the curing behavior of BCB and/or vinyl groups, ensuring adaptability to diverse processing conditions. More importantly, all the cured cPI-BCB, cPI-cBCB, and HPI-cBCB films demonstrated $D_k < 2.5$ and $D_f < 5 \times 10^{-3}$ (at 1 MHz). These results highlighted that the synergistic effect between the BCB and vinyl functional groups has greatly facilitated PI with promising potential as a novel interlayer dielectric material for 5G applications.

ASSOCIATED CONTENT

Supporting Information

The Supporting Information is available free of charge at https://pubs.acs.org/doi/10.1021/acs.macromol.5c02864.

Experimental details and additional characterization data, including ^{1}H NMR spectra, comparison of the dielectric constant (D_k) and dissipation factor (D_f), images of the PI-cBCB-20 film, cross-linking density data, and performance parameters (PDF)

AUTHOR INFORMATION

Corresponding Author

Guowei Wang − *State Key Laboratory of Molecular Engineering of Polymers, Department of Macromolecular Science, Fudan University, Shanghai 200433, China;*

https://doi.org/10.1021/acs.macromol.5c02864
Macromolecules 2025, 58, 13373−13381

orcid.org/0000-0003-2595-8269; Email: gwwang@fudan.edu.cn

Authors

Chengcheng Zhou − *State Key Laboratory of Molecular Engineering of Polymers, Department of Macromolecular Science, Fudan University, Shanghai 200433, China*

Ding Shen − *State Key Laboratory of Molecular Engineering of Polymers, Department of Macromolecular Science, Fudan University, Shanghai 200433, China*

Boyang Shi − *State Key Laboratory of Molecular Engineering of Polymers, Department of Macromolecular Science, Fudan University, Shanghai 200433, China*

Xiaotong Fang − *State Key Laboratory of Molecular Engineering of Polymers, Department of Macromolecular Science, Fudan University, Shanghai 200433, China*

Xingpeng Chai − *State Key Laboratory of Molecular Engineering of Polymers, Department of Macromolecular Science, Fudan University, Shanghai 200433, China*

Complete contact information is available at: https://pubs.acs.org/10.1021/acs.macromol.5c02864

Notes

The authors declare no competing financial interest.

■ ACKNOWLEDGMENTS

This work is supported by the National Natural Science Foundation of China (22271058).

■ REFERENCES

(1) Hatton, B. D.; Landskron, K.; Hunks, W. J.; Bennett, M. R.; Shukaris, D.; Perovic, D. D.; Ozin, G. A. Materials chemistry for low-k materials. *Mater. Today* **2006**, *9* (3), 22−31.

(2) Maier, G. Low dielectric constant polymers for microelectronics. *Prog. Polym. Sci.* **2001**, *26* (1), 3−65.

(3) Shamiryan, D.; Abell, T.; Iacopi, F.; Maex, K. Low-k dielectric materials. *Mater. Today* **2004**, *7* (1), 34−39.

(4) Volksen, W.; Miller, R. D.; Dubois, G. Low dielectric constant materials. *Chem. Rev.* **2010**, *110* (1), 56−110.

(5) Yuan, C.; Jin, K. K.; Li, K.; Diao, S.; Tong, J. W.; Fang, Q. Nonporous low-k dielectric films based on a new structural amorphous fluoropolymer. *Adv. Mater.* **2013**, *25* (35), 4875−4878.

(6) Maier, J. Nanoionics: ion transport and electrochemical storage in confined systems. *Nat. Mater.* **2005**, *4* (11), 805−815.

(7) Hou, J. R.; Fang, L. X.; Huang, G.; Dai, M. L.; Liu, F. P.; Wang, C. Y.; Li, M. H.; Zhang, H.; Sun, J.; Fang, Q. Low-dielectric polymers derived from biomass. *ACS Appl. Polym. Mater.* **2021**, *3* (6), 2835−2848.

(8) Huang, G.; Sun, J.; Fang, Q. Thermo-crosslinkable molecular glasses towards the low k materials at high frequency. *Mater. Today Chem.* **2022**, *24*, 100782.

(9) Hu, Z. D.; Liu, X. Q.; Ren, T. L.; Saeed, H. A. M.; Wang, Q.; Cui, X.; Huai, K.; Huang, S. H.; Xia, Y. M.; Fu, K.; Zhang, J. M.; Chen, Y. W. Research progress of low dielectric constant polymer materials. *J. Polym. Eng.* **2022**, *42* (8), 677−687.

(10) Xie, M.; Li, M. L.; Sun, Q.; Fan, W. J.; Xia, S.; Fu, W. X. Research progress on porous low dielectric constant materials. *Mater. Sci. Semicond. Process.* **2022**, *139*, 106320.

(11) Zhou, J. F.; Tao, Y. Q.; Chen, X. Y.; Chen, X. R.; Fang, L. X.; Wang, Y. Q.; Sun, J.; Fang, Q. Perfluorocyclobutyl-based polymers for functional materials. *Mater. Chem. Front.* **2019**, *3* (7), 1280−1301.

(12) Wang, J. J.; Jin, K. K.; Sun, J.; Fang, Q. Dendrimeric organosiloxane with thermopolymerizable -OCF = CF_2 groups as the arms: synthesis and transformation to the polymer with both ultra-low k and low water uptake. *Polym. Chem.* **2016**, *7* (20), 3378−3382.

(13) Babb, D. A.; Ezzell, B. R.; Clement, K. S.; Richey, W. F.; Kennedy, A. P. Perfluorocyclobutane aromatic ether polymers. *J. Polym. Sci., Part A:Polym. Chem.* **1993**, *31* (13), 3465−3477.

(14) Wang, J. J.; Zhou, J. F.; Jin, K. K.; Wang, L.; Sun, J.; Fang, Q. A new fluorinated Polysiloxane with good optical properties and low dielectric constant at high frequency based on easily available tetraethoxysilane (TEOS). *Macromolecules* **2017**, *50* (23), 9394−9402.

(15) Grosso, D.; Boissière, C.; Sanchez, C. Ultralow-dielectric-constant optical thin films built from magnesium oxyfluoride vesicle-like hollow nanoparticles. *Nat. Mater.* **2007**, *6* (8), 572−575.

(16) Seino, M.; Wang, W. D.; Lofgreen, J. E.; Puzzo, D. P.; Manabe, T.; Ozin, G. A. Low-k periodic mesoporous organosilica with air walls: POSS-PMO. *J. Am. Chem. Soc.* **2011**, *133* (45), 18082−18085.

(17) Fu, G. D.; Yuan, Z. L.; Kang, E. T.; Neoh, K. G.; Lai, D. M.; Huan, A. C. H. Nanoporous ultra-low-dielectric-constant fluoropolymer films via selective UV decomposition of poly(pentafluorostyrene)-block-poly(methyl methacrylate) copolymers prepared using atom transfer radical polymerization. *Adv. Funct. Mater.* **2005**, *15* (2), 315−322.

(18) Fu, G. D.; Shang, Z. H.; Hong, L.; Kang, E. T.; Neoh, K. G. Nanoporous, ultralow-dielectric-constant fluoropolymer films from agglomerated and crosslinked hollow nanospheres of poly(pentafluorostyrene)-block-poly(divinylbenzene). *Adv. Mater.* **2005**, *17* (21), 2622−2626.

(19) Evans, A. M.; Giri, A.; Sangwan, V. K.; Xun, S. N.; Bartnof, M.; Torres-Castanedo, C. G.; Balch, H. B.; Rahn, M. S.; Bradshaw, N. P.; Vitaku, E.; Burke, D. W.; Li, H.; Bedzyk, M. J.; Wang, F.; Brédas, J. L.; Malen, J. A.; McGaughey, A. J. H.; Hersam, M. C.; Dichtel, W. R.; Hopkins, P. E. Thermally conductive ultra-low-k dielectric layers based on two-dimensional covalent organic frameworks. *Nat. Mater.* **2021**, *20* (8), 1142−1148.

(20) Zhou, D. L.; Li, J. H.; Guo, Q. Y.; Lin, X.; Zhang, Q.; Chen, F.; Han, D.; Fu, Q. Polyhedral oligomeric silsesquioxanes based ultralow-k materials: The effect of cage size. *Adv. Funct. Mater.* **2021**, *31* (31), 2102074.

(21) Fan, W. J.; Hong, N. M.; Sun, Q.; Li, M. L.; Fu, W. X. Thermocurable and photo-patternable polysiloxanes and polycarbosiloxanes by a facile Piers-Rubinsztajn polycondensation and post-modification. *Polym. Chem.* **2022**, *13* (15), 2187−2194.

(22) Kong, L. Q.; Cheng, Y. R.; Jin, Y. X.; Ren, Z. D.; Li, Y.; Xiao, F. Adamantyl-based benzocyclobutene low-k polymers with good physical properties and excellent planarity. *J. Mater. Chem. C* **2015**, *3* (14), 3364−3370.

(23) Fan, L.; Peng, Q. X.; Yuan, W.; Li, X.; Hu, H.; Ma, J. J.; Huang, Y. W.; Yang, J. X. UV-curable low dielectric siloxane-benzocyclobutene resins via introducing carbosilane groups. *Eur. Polym. J.* **2021**, *161*, 110833.

(24) Meng, S. M.; Liao, D. H.; Li, C.; Xu, M. H. Synthesis of partially fluorinated polyolefins via copolymerization of ethylene with fluorinated norbornene-based comonomers. *Polym. Chem.* **2024**, *15* (16), 1642−1647.

(25) Mural, P. K. S.; Kumar, B.; Madras, G.; Bose, S. Chitosan immobilized porous polyolefin as sustainable and efficient antibacterial membranes. *ACS Sustainable Chem. Eng.* **2016**, *4* (3), 862−870.

(26) Takeuchi, D.; Nakamura, M.; Osakada, K. Copolymerisation of 1-alkenes with bulky oxygen-containing olefins for dual-stage functionalisation of polyolefins. *Polym. Chem.* **2021**, *12* (2), 299−306.

(27) Han, K. K.; Zhou, J.; Li, Q. Z.; Shen, J.; Qi, Y. Y.; Yao, X. P.; Chen, W. Effect of filler structure on the dielectric and thermal properties of SiO_2/PTFE composites. *J. Mater. Sci.:Mater. Electron.* **2020**, *31* (12), 9196−9202.

(28) Li, C. P.; Ji, S. N.; Jiang, X. H.; Waterhouse, G. I. N.; Zhang, Z. M.; Yu, L. M. Microwave absorption by watermelon-like microspheres composed of γ-Fe_2O_3, microporous silica and polypyrrole. *J. Mater. Sci.* **2018**, *53* (13), 9635−9649.

(29) Pálvölgyi, P. S.; Nelo, M.; Pitkänen, O.; Peräntie, J.; Liimatainen, H.; Myllymäki, S.; Jantunen, H.; Kordas, K. Ultra-low

permittivity porous silica-cellulose nanocomposite substrates for 6G telecommunication. *Nanotechnology* **2020**, *31* (43), 435203.
(30) Gu, J. W.; Meng, X. D.; Tang, Y. S.; Li, Y.; Zhuang, Q.; Kong, J. Hexagonal boron nitride/polymethyl-vinyl siloxane rubber dielectric thermally conductive composites with ideal thermal stabilities. *Composites, Part A* **2017**, *92*, 27−32.
(31) Takahashi, S.; Imai, Y.; Kan, A.; Hotta, Y.; Ogawa, H. Dielectric and thermal properties of isotactic polypropylene/hexagonal boron nitride composites for high-frequency applications. *J. Alloys Compd.* **2014**, *615*, 141−145.
(32) Wu, B.; Xu, Y.; Wu, N.; Tang, X. Z. Effect of surface functionalized SiO_2 particles filled polyolefin on the dielectric properties of laminates. *Eur. Polym. J.* **2021**, *155*, 110570.
(33) Wu, B.; Mao, X.; Xu, Y.; Li, R.; Wu, N.; Tang, X. Z. Improved dielectric and thermal properties of core-shell structured SiO_2/polyolefin polymer composites for high-frequency copper clad laminates. *Appl. Surf. Sci.* **2021**, *544*, 148911.
(34) Wu, L. C.; Wang, L.; Wang, J. Fractures of low-k materials in a RF package with integrated passive device based on TGV. *Microelectron. Eng.* **2024**, *291*, 112195.
(35) Garea, S. A.; Corbu, A. C.; Deleanu, C.; Iovu, H. Determination of the epoxide equivalent weight (EEW) of epoxy resins with different chemical structure and functionality using GPC and ^{1}H-NMR. *Polym. Test.* **2006**, *25* (1), 107−113.
(36) Luk, S. B.; Métafiot, A.; Morize, J.; Edeh, E.; Maric, M. Hydrogenation of poly(myrcene) and poly(farnesene) using diimide reduction at ambient pressure. *J. Polym. Sci.* **2021**, *59* (19), 2140−2153.
(37) Zhou, C. C.; Shen, D.; Chai, X. P.; Shi, B. Y.; Zhu, W. Y.; Wang, G. W. A low dielectric constant material synergized by calix[4]arene and benzocyclobutene units. *J. Mater. Chem. C* **2023**, *11* (31), 10509−10519.
(38) Li, M. H.; Sun, J.; Fang, Q. Low dielectric constant polymers derived from bio-based anethole and isoeugenol. *Eur. Polym. J.* **2024**, *202*, 112639.
(39) Zhang, H.; Sun, J.; Fang, Q. A low dielectric polymer with high thermostability derived from bio-based isoeugenol. *Eur. Polym. J.* **2022**, *179*, 111527.
(40) Maier, G. The search for low-ε and ultra-low-ε dielectrics: how far can you get with polymers? Part 1: Background. *IEEE Electr. Insu.l M.* **2004**, *20* (2), 6−17.

https://doi.org/10.1021/acs.macromol.5c02864
Macromolecules 2025, 58, 13373−13381